Modelling Glacier Evolution in Bhutanese Himalaya during the Little Ice Age

Weilin Yang[1], Yingkui Li[2], Gengnian. Liu[1], Wenchao Chu[3]

[1]College of Urban and Environmental Sciences, Peking University, Beijing 100871, China.

[2]Department of Geography, University of Tennessee, Knoxville, TN 37996, USA.

[3]Department of Earth System Science, Ministry of Education Key Laboratory for Earth System Modeling, Institute for Global Change Studies, Tsinghua University, Beijing 100084, China.

Correspondence to: Wenchao Chu (peterchuwenchao@foxmail.com)

Abstract. Mountain glaciers provide us a window into past climate change and landscape evolution, but the pattern of glacier evolution at centennial or suborbital timescale remains elusive, especially in monsoonal Himalayas. We simulated the glacier evolution in Bhutanese Himalaya, a typical monsoon influenced region, during the Little Ice Age (LIA), using the Open Global Glacier Model and six paleo-climate datasets. Compared with the mapped glacial landforms, the model can well capture the glacier length changes, especially for the experiment driving by the GISS climate dataset, but overestimates the changes in glacier area. Simulation results reveal four glacial substages at 1270s-1400s, 1470s-1520s, 1700s-1710s, and 1820s-1900s in the study area. From further analysis, a negative correlation between the number of the substages and glacier length was found, which suggests that the number and occurrence of glacial substages are regulated by the heterogeneous responses of glaciers to climate change. In addition, the changes in summer temperature dominated the glacier evolution in this region during the LIA.

1 Introduction

Mountain glaciers over high Himalayas provide us a critical window to explore the linkage between climatic, tectonic, and glacial systems (Oerlemans et al., 1998; Owen et al., 2009; Dortch et al., 2013; Owen & Dortch, 2014; Saha et al., 2018). Many scientists have investigated the glacial history for Himalayas at orbital-scale, indicating that a general trend of glacier advances is related to overall summer temperature, forced by orbitally-controlled insolation (Murari et al., 2014; Yan et al., 2018, 2020, 2021). However, latest observations with finer temporal resolution have revealed that the evolution of some glaciers in monsoonal Himalayas has suborbital-scale fluctuations, which has aroused more and more interest on exploring the mechanisms behind (Solomina et al., 2015; Peng et al., 2020).

The Little Ice Age (LIA; from 1300 to 1850 CE; Grove, 2013; Qureshi et al., 2021) is the latest cooling event during the Holocene, during which most mountain glaciers advanced, forming abundant well-preserved and distinctive geomorphic landforms (Murari et al., 2014; Qiao & Yi, 2017; Peng et al., 2019, 2020). Previous studies have reconstructed the timing and extent of glacier evolution during the LIA based on field investigation, geomorphological mapping, and cosmogenic nuclide

31   dating (Owen & Dortch, 2014 and references therein; Zhang et al., 2018a, 2018b; Carrivick et al., 2019; Qureshi et al., 2021).

32   However, dating glacial landform is challenging due to the post glacial degradation and the large uncertainties in the dating

33   methods (Heyman et al., 2011; Fu et al., 2013). In addition, the reconstructions using individual glaciers or a small number of

34   glaciers may be not representative for the regional average (Carrivick et al., 2019). It is therefore still unclear on how many

35   substages exist during the LIA and how to separate the contribution of precipitation and temperature on glacier evolution.

36   Numerical glacial modelling is a powerful way to study glacier evolution on centennial timescale (Parkes & Goosse, 2020)

37   and quantify the response of glaciers to climate change (Eis et al., 2019). The modelling approach can largely alleviate the

38   limitations of field-based methods in exploring response of glaciers to climate change on the regional scale and provides an

39   opportunity to understand the pattern of glacier change during the LIA. The model simulation can be cross validated using

40   multiple observational records. However, evaluating the simulation results is still challenging due to the scarcity of the direct

41   observational record for glacier changes during the LIA (Goosse et al., 2018).

42   The ongoing debate about the pattern of glacier evolution during the LIA is, in part, resulted from an imperfect

43   understanding on how to cross validate observation with simulation, what the contribution of individual glacier to regional

44   glacier evolution is, and how climate change drives glacier evolution (Goosse et al., 2018; Carrivick et al., 2019; Peng et al.,

45   2019, 2020). Based on previous works, this study improves the understanding of the pattern of LIA glacier changes in

46   Bhutanese Himalaya (BH; Fig. 1), a typical monsoon-influenced area, using the Open Global Glacier Model (OGGM). We

47   systematically simulated the glacier changes during the LIA based on the climate data from six different general circulation

48   models (GCMs). The simulated changes in glacier length, area and equilibrium line altitude (ELA) are validated by

49   geomorphological maps and previous studies. The pattern of regional glacial evolution is compared with [10]Be glacial

50   chronologies across the monsoon influenced Himalayas. The dominant climatic factors of the regional glacial evolution are

51   explored through a series of sensitivity experiments.
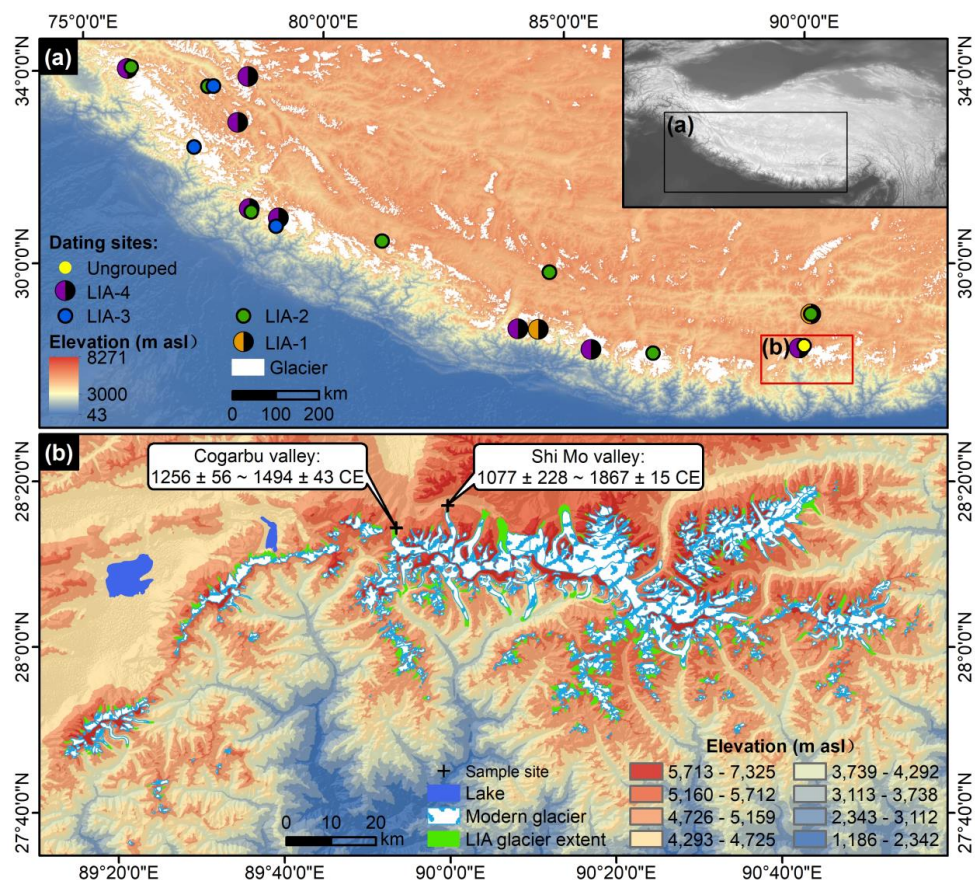
Figure 1. (a) The distribution of the ¹⁰Be surface exposure dating sites in monsoonal Himalayas. The ¹⁰Be surface exposure ages are
recalculated using CRONUS Earth V3 online calculator (Balco et al., 2008; http://hess.ess.washington.edu/math/) and the moraine
ages are determined based on the criterion in Peng et al. (2019) (see Text S1, Table S1 and Fig. S1 for details). (b) Mapped 408 glaciers
during the LIA and the contemporary periods. The ages of the LIA moraines in BH are from Peng et al. (2019, 2020).

2 Methods

2.1 The Open Global Glacier Model

The OGGM is a 2D ice-flow model, to simulate past and future mass-balance, volume, and geometry of glaciers
(Maussion et al., 2019). Studies indicated that a good performance of this model in simulating alpine glaciers (Farinotti et al.,
2017; Pelto et al., 2020) and reproducing the millennial trend of glacial evolution in mountainous regions (Goosse et al., 2018;
Parkes & Goosse, 2020).

The OGGM couples a surface mass balance (SMB) scheme with a dynamic core. The dynamic core is based on the
shallow-ice approximation (SIA), computing the depth-integrated ice flux of each cross-section along multiple connected
flowlines that are diagnosed from a pre-process algorithm. The spatial resolution (dx; m) of the target grid is scale dependent,
determined by the size of the glacier ($dx=14S^{\frac{1}{2}}+10$, with S representing the glacier area in km²) and a predefined minimum (10

67   m) and maximum (200 m) values, respectively (Bahr et al., 2014). The ice accumulation is estimated by a solid precipitation

68   scheme to separate the total precipitation into rain and snow based on monthly air temperature. In this scheme, the amount of

69   solid precipitation is computed as a fraction of the total precipitation. Specially, precipitation is entirely solid if $T_i <= T_{Solid}$

70   (default setting is 0 °C), entirely liquid if $T_i >= T_{Liquid}$ (defaults to 2 °C) or divided into solid and liquid parts based on a linear

71   relationship with those two temperature values. The ablation is estimated using a positive degree-day (PDD) scheme (Eq. 1).

72   Melting occurs if monthly temperature ($T_i(z)$) is above T_{melt}, which is equal to -1 °C.

73    $$m_i(z) = p_f P_i^{solid}(z) - \mu^* \cdot max(T_i(z) + \beta - T_{melt}, 0) + \varepsilon,$$ (1)

74   where $m_i(z)$ is the monthly SMB at elevation z of month i. $P_i^{solid}(z)$ is the monthly solid precipitation, and P_f is a general

75   precipitation correction factor (default setting is 2.5). β is the temperature bias (defaults to 0 °C) and a residual bias term (ε) is

76   added as a tuning parameter to represent the collective effects of non-climate factors. Different from the conventional PDD

77   schemes embedded in other ice sheet models, such as Parallel Ice Sheet Model (Bueler & Brown, 2009; Winkelmann et al.,

78   2011), SICOPOLIS (Greve, 1997a, 1997b) or CISM (Lipscomb et al., 2019), that assume ε and μ^* as constant values, these

79   parameters vary with glacier in OGGM to better capture the changes of individual glaciers.

80   **2.2 Climate forcing and experimental design**

81   The temperature and precipitation datasets from six different GCMs (BCC-CSM, CCSM4, CESM, GISS, IPSL, MPI)

82   were used as climate forcing to drive OGGM. These data are available in the Past Model Intercomparison Project (PMIP3)

83   and the Coupled Model Intercomparison Project (CMIP5) protocols (Schmidt et al., 2011; Tayloret al., 2012; PAGES 2k-

84   PMIP3 group, 2015) – with details listed in Goosse et al. (2018) and Table S2. The climate data cannot be directly used in

85   glacial model due to the systematical bias in the climate datasets produced by different GCMs. A calibration algorithm is

86   adopted by OGGM to correct the GCMs climate data series by taking the anomalies between GCMs and the CRU TS 4.01

87   mean climate from 1961 to 1990 (Parkes et al., 2020).

88   To better estimate the long-term glacier evolution for each GCM forcing, the spin-up procedures and parameter tunning

89   are required to initiate the model, because the model is sensitive to the initial condition (Eis et al., 2019). A 600-year spin-up

90   is conducted using annual climate data selected randomly from a 51-year window of 875-925 CE from the corresponding GCM

91   prior to the long-term integrations. The tunable parameter, β, in Equation S1 is set as -1°C based on a set of sensitivity tests in

92   which we adjust β from -1 to 1 °C with an increment of 1 °C. We found that simulation results of the first ~250 years are

93   sensitive to β that larger β will lead to smaller glacier initial state, but such sensitivity rapidly diminishes in the long-term

94   simulation. Thus, the only criterion for we to tune β is to ensure the LIA start time close to the [10]Be chronologies in BH. After

95   spin-up, the simulations are conducted during the period of 900-2000 CE for all glacial evolution experiments. Because the

96   simulation of the first 100 years (900-1000 CE) is influenced by the choice of initial conditions, we limit our analyses to the

97   simulations in 1000-2000 CE to examine the glacier response to climate trends (Goosse et al., 2018; Parkes, et al., 2020).

98   We also test the sensitivity of glaciers to temperature and precipitation through control experiments. We apply a 'constant

99   climate scenario', use the CRU datasets as the climate forcing, and run the simulation until reaching equilibrium (piControl).

100   The window size is set to 51-year and centered on t^*, the year for which the surface mass balance (SMB) scheme best

101   reproduces the observed SMB. We set ε to 0 in Eq. 1, in order to maintain the contemporary glacier geometry under the

102   contemporary climate condition. Then, keeping the same precipitation, stepwise changes (at 0.1 °C) in annual temperature

103   from -1 to 1 °C are uniformly added to the CRU datasets to test the sensitivity of temperature on glacier evolution. The similar

104   analysis is conducted to test the sensitivity of precipitation by keeping the same temperature record and adjusting precipitation

105   from -20 to 20 % with an increment of 2 %. In addition, we did similar control experiments to explore the sensitivity of

106   temperature and precipitation in different seasons.

2.3 Establishing Regional Chronology and Mapping LIA Glacier

108   The simulated timing and extent of glacial advances are validated with the [10]Be surface exposure ages of the LIA moraines

109   and the mapping of LIA glaciers over BH. Previous studies have dated some well-preserved moraine sequences to represent

110   the time of regional glacial advances during the LIA. Five [10]Be ages from moraine M1 of Cogarbu valley and seven [10]Be ages

111   from moraine M1 of Shi Mo valley were chosen to determine the regional glaciation chronology establishing in BH (Fig. 1b

112   and Fig. S1). We also chose 126 [10]Be surface exposure ages across the monsoonal Himalayas for regional chronological

113   comparison (Table S1). The criteria of [10]Be surface exposure ages and moraine ages recalculated are shown in Text S1.

114   Based on regional glacial chronology and the evidence of sediment-landform assemblages (Chandler et al., 2019), we

115   map the lateral and terminal moraines in BH to represent the maximum extent of glaciers during the LIA. The LIA moraines

116   are usually well-preserved with sharp crests, distributed several hundred meters to a few kilometers away from the termini of

117   modern glaciers, and damming a lake in front of modern glaciers (Zhang et al., 2018b; Qureshi et al., 2021). We use the world

118   imagery ESRI (http://goto.arcgisonline.com/maps/World_Imagery) and Google Earth high-resolution imagery to delineate the

119   outlines of LIA glaciers based on the LIA moraines. We also downloaded their corresponding contemporary glaciers from

120   Randolph Glacier Inventory V6 datasets (RGI; RGI Consortium, 2017). The area and length of contemporary glaciers are

121   provided in RGI datasets. We calculated the area and the length (using the length of the main flowline) of the LIA glaciers in

122   ArcGIS.

3 The pattern of glacier changes during the LIA

124   We simulated the continuous response of glaciers to climate change in BH during the LIA using OGGM. Large deviations

125   exist among the simulations using the BCC-CSM, CCSM4, and CESM climate datasets in comparison with the observations

126   (Fig. S2). The simulation based on the CESM climate forcing dataset showed the BH was always ice free during the last

127   millennium due to high temperature, inconsistent with the fact that glaciers still exist in this area even now. For the BCC-CSM

128   and CCSM4 climate datasets, we found an extraordinary rising in temperature after the 1850s, leading to an unreasonably

129   retreat of glaciers so that the modern glacier extent was far less than observations. These three simulations excessively

130   overestimated the amplitude of glacier changes. Thus, we removed these simulations from the discussion and only focused on

131   the pattern of glacier changes during the LIA based on the simulations of the GISS, IPSL, and MPI experiments.

132   Similar to previous studies (Goosse et al., 2018; Parkes & Goosse, 2020), we used the glacier length to analyze glacier

133   evolution and evaluate the climate model performance. Four substages (glacial advances) are identified in the GISS, IPSL, and

134   MPI experiments (marked as LIA-4 to LIA-1 from old to young). Fig. 2 and Table S3 illustrate their occurrences, and changes

135   in glacier length, area, and volume.

136   The simulations for the GISS experiment indicate that the most extensive valley and piedmont glaciers occurred during

137   the early LIA (LIA-4), around 1400s. The total glacier length, area, and volume during LIA-4 were 72.9 %, 175.0 %, and

138   465.7 % larger than the present, respectively. The second most extensive glacial advance occurred during LIA-3 (about 1520s),

139   following by LIA-1 (about 1880s). The smallest glacial advance (LIA-2) occurred about 1700s with the glacier length, area,

140   volume changes of 37.9 %, 127.8 %, and 354.7 %, respectively.

141   Similar to the GISS experiment, the maximum changes in glacier length (about 97.6 %), area (about 221.9 %), volume

142   (589.7 %) occurred during LIA-4 for the IPSL experiment. However, the occurrence of LIA-4 in the IPSL experiment (1330s)

143   was older than that in the GISS experiment (about 1400s). The second most extensive glacial advance occurred during LIA-2

144   (about 1710s) for the climate forcing of IPSL dataset, different from the results of the GISS experiment. The minimum glacial

145   advance occurred during LIA-1 (about 1900s) with the glacier length of 56.4 % longer and the glacier area and volume of

146   128.9 % and 342.2 % larger than the present, respectively.

147   These four substages (LIA-4 to LIA-1) occurred at about 1270s, 1470s, 1700s, and 1820s in the MPI experiment,

148   respectively. Focused on the glacier length changes, the most extensive glacial advances occurred during LIA-4 with a glacier

149   length of 117.7 % longer than the present, following by LIA-3, LIA-1, and LIA-2 with 76.6 %, 70.9 %, and 61.7 % longer in

150   glacier length than the present, respectively.

151

152
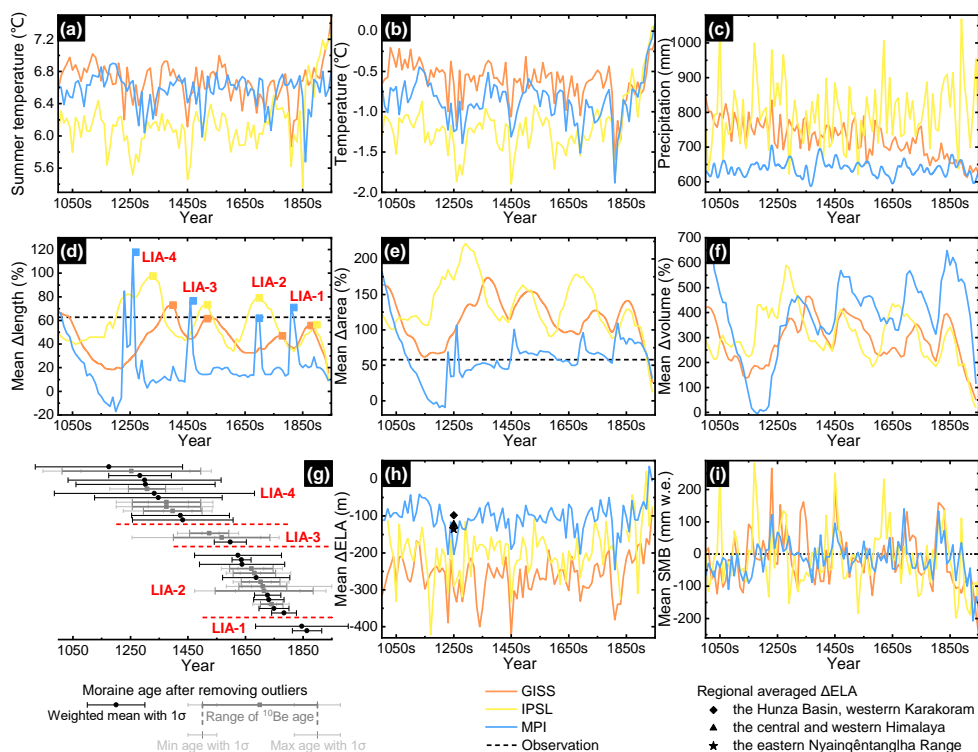
Figure 2. Interannual (a) summer temperature, (b) temperature, and (c) precipitation changes from 1000s to 1950s averaged over
Bhutanese Himalaya. Glacier (d) length, (e) area, (f) volume, (h) ELA, and (i) SMB changes during LIA across the studied area,
modelled by OGGM using three separate GCM produces (GISS, IPSL, and MPI). Each glacier in the OGGM runs has its length,
area, volume, and ELA changes normalized relative to the corresponding averaged parameters during 1950s in the run output.
Besides, the recalculated moraine ages across the monsoon-influenced Himalaya are also shown (g). The regional averaged ΔELAs
are illustrated in Fig. 2h.

4 Discussions

4.1 The Comparison between Simulations and Observations

We validated the simulation results using mapped LIA glaciers. The regional average length of 408 mapped LIA glaciers
is about 62.7 % longer than the present glaciers along the flowlines, similar to the simulation results of the GISS experiment
(72.9 %). Simulations with IPSL (97.6 %) and MPI (117.7 %) datasets overestimated the length change of LIA glaciers. A
possible explanation for the overestimation of the IPSL and MPI experiments is that the larger amplitude of temperature
reduction causes the sharply increasing of positive SMB, leading to the intensively glacier advance during the glacial period.

All of three experiments overestimate the area of LIA glaciers in comparison with the mapped moraines and the studies
from nearby area. The mapped total LIA glacier area is about 57.9 % larger than the present value, which is significantly
smaller than the simulated 175.0 % for the GISS experiment, 221.9 % for the IPSL experiment, and 109.6 % for the MPI
experiment. At the regional scale, the total glacier area has increased about 45.3 % during LIA in the central and western

170 Himalayas relative to that in 2015 (Qiao & Yi, 2017), and 81.2 % during LIA in the Gangdise Mountains relative to that in

171 2010 (Zhang et al., 2018b) based on the glacial geomorphological maps. The overestimated of the area change of LIA glaciers

172 is likely caused by two reasons: 1) OGGM is a flowline-based model and the model-derived flowline becomes less valid when

173 glaciers expended to large and complex glaciers (Maussion et al., 2019); and 2) when tributary glaciers merge into a main

174 glacier, OGGM calculates the areas of the tributary and main glaciers repeatedly, overestimating the glacier area (Goosse et

175 al., 2018). The simulated glacier volume further amplified the differences with the overestimated glacier areas as the volume

176 equals to the product of the area and the thickness.

177   Compared with previous investigations, the model simulates the ΔELA quite well for the MPI experiment but

178 overestimates the ΔELA for GISS and IPSL experiments (Fig. 2h; Loibl et al., 2014; Qiao & Yi, 2017; Qureshi et al., 2021).

179 ELA is the elevation where accumulation equals ablation for a certain glacier (Eq. 1; Benn & Lehmkuhl, 2000; Heyman, 2014).

180 The larger positive SMB makes the glacier advanced and the ELA dropped. Thus, the amplitude of ΔELA is determined by

181 the amplitude of SMB. It seems that the GISS and IPSL climate datasets caused dramatic changes in SMB and higher ELA.

182   Above all, different climate datasets have different performances for different parameters. The GISS climate dataset

183 performs better for the glacier length change, but the MPI better for the ELA change.

184 4.2 Why exists four LIA substages in BH?

185   Although large uncertainties exist in cosmogenic nuclide surface exposure dating, it is still one of main methods to

186 constrain the glacial chronology. Many studies have been conducted in dating the LIA moraines in or nearby our simulation

187 region (Fig. 2g and Table S1). However, the dating results vary with glaciers. For example, only one moraine was dated in

188 Cogarbu valley (1256 ± 56 - 1494 ± 43 CE; Fig. S1; Peng et al., 2019), but two substages were constrained in Lato valley,

189 Lahul Himalaya (Saha et al., 2018), Langtang Khola valley, Nepal Himalaya (Barnard et al., 2006), and Gongotri Ganga valley,

190 Garhwal Himalaya (Barnard et al., 2004). Liu et al. (2017) have found at least three LIA moraines in Lhagoi Kangri Range,

191 Karola Pass. Murari et al. (2014) and Zhang et al. (2018a) have identified at least four LIA moraines in Bhillangana and

192 Dudhganga valleys, Garwal Himalaya, and Lopu Kangri Area, central Gangdise Mountains, respectively. The difference in

193 LIA substages has been explained by the different climate conditions in these areas (Owen & Dortch, 2014; Murari et al., 2014;

194 Saha et al., 2019).

195   We argue that the difference in LIA substages is caused by the sensitivity of different glaciers rather than the regional

196 climate conditions. We found a negative correlation between the number of LIA substages and the length of glaciers in BH

197 (the correlation coefficients are -0.21, -0.32, and -0.33 for the GISS, IPSL, and MPI experiments, respectively; Fig. 3a and Fig.

198 3b), indicating that smaller glaciers are more sensitive to climate change compared to larger glaciers (Xu et al., 2011). As

199 illustrated by the frequency of the number of LIA substages of each glacier (Fig. 3b), about 42.1 % of glaciers for the GISS

200 experiment, 60.8 % of glaciers for the IPSL experiment, and 62.0 % of glacier for the MPI experiment have four LIA substages.

201   Except for the simulation results of the GISS experiment (1364 m), the average length of the glaciers with four LIA substage

202   was about 1628 and 1613 m for the IPSL and MPI experiments, respectively, consistent with the regional average length of

203   modern glaciers (1596 m; Fig. 3a).

204
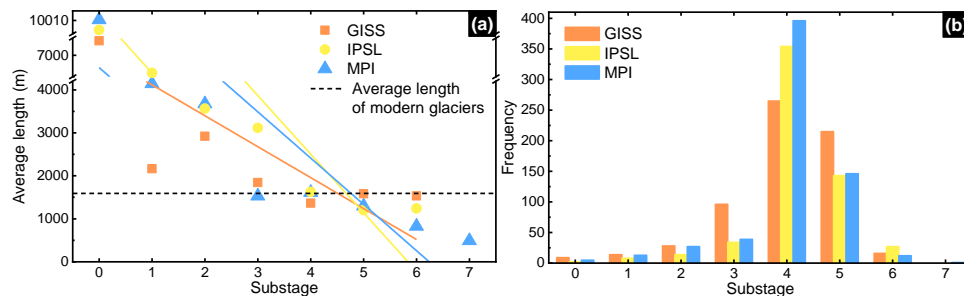
206   **Figure 3. (a) The relationship between the number of substages and the average glacier length of each substage. (b) The frequency**
207   **distribution chart shows the number of the LIA substages of each glacier.**

208   The number of preserved substages is influenced by the extent of glacial advance in each substage. If the extent of glacial

209   advance is larger during the later substage, the early glacial landforms would be destroyed by glacial advance, causing the lack

210   of earlier substages (Li et al., 2011; Fu et al., 2013). For example, we expect that most moraines will be found during LIA-4,

211   LIA-3, and LIA-1 in the field investigation if the climate follows the GISS and MPI experiments scenario, but lack of the

212   moraines during LIA-2 because of its limited extent of glacier advance than LIA-1. In contrast, most of moraines should be

213   dated to LIA-4, LIA-2, and LIA-1 under the IPSL experiment scenario. Most available [10]Be ages concentrated in LIA-4 and

214   LIA-2 (13 and 14 moraines were dated to LIA-4 and LIA-2, respectively; Fig. 2g), indicating that the IPSL experiment captured

215   glacial fluctuations during the LIA (Fig. 2d).

216   A small number of moraines were dated to LIA-3, such as the moraine m_{bd2} and moraine m_{bk2} in Garhwal Himalaya

217   (Murari et al., 2014) and moraine m_{A2c} in Lato valley (Saha, et al., 2018), indicating that not all glaciers advanced to their

218   second longest length during LIA-2 (the IPSL experiment; Fig. 2d). Our simulations also support this observation. As

219   illustrated in Fig. S4, about 49.0 % of glaciers occurred during LIA-2 and 25.5 % of glaciers occurred during LIA-3. If the

220   dated moraine belongs to these 25.5 % glaciers, the glacier advance would be found. Similarly, not all glaciers advanced to

221   their longest length during the early LIA (LIA-4). For the IPSL experiment, about 98.1 % of glaciers have the longest length

222   during LIA-4, but it is more complex for the simulation results driven by the GISS and MPI climate datasets (Fig. S4). For the

223   MPI experiment, about 80.4 % glaciers advanced most extensive during LIA-4, but there were still about 12.9 % of glaciers

224   have the maximum glacier length change after 1800s (Fig. S5). For the GISS experiment, these two numbers were 47.2 % and

225   29.3 % (Fig. S3). If we chose the glaciers which reached their most extensive glacial advance after 1800s, the glacial landforms

226   before 1800s would be destroyed.

227   In summary, the regional glacial evolution is a collective effect of individual glacier changes. Four substages during LIA

228   at the regional scale does not guarantee that each individual glacier has four substages. Instead, it only represents the

229   characteristics of most typical glaciers that accounted for the vast majority of the total glaciers. This can explain why there

230   exists four substages in regional scale in the simulation but is hard captured in the previous studies that only focus on one

231   individual glacier, which helps us to deeply understand the relationship between regional glacial evolution and the individual

232   glacier response to climate change.

233   **4.3 Climate-forcing Mechanisms**

234   Positive or negative SMB determines whether a glacier advances or retreats, and the amplitude of glacier change is

235   directly influenced by the amplitude of SMB change and the duration of the positive or negative SMB (Marzeion et al., 2012;

236   Maussion et al., 2019; Fig. 2i). Previous studies indicated that the change of SMB is determined by the temperature and

237   precipitation change according to the PDD scheme and the climatic proxy comparison (Eq. 1; Fig. 2a-2c; Marzeion et al., 2012;

238   Maussion et al., 2019; Peng et al., 2019, 2020; Parkes, et al., 2020). Our study revealed that the summer temperature plays a

239   dominant role in controlling glacier changes at suborbital-scale.

240   Figure 4 illustrates the average monthly temperature, precipitation and ΔSMB for the GISS, IPSL, and MPI experiments

241   during LIA and at present. For these three experiments, the magnitudes of SMB changes in summer are about 224, 167, and

242   113 mm w.e., accounting for 82.6 %, 71.8 %, and 85.2 % to the annual ΔSMB, respectively, indicating that the summer climate

243   condition dominants the change of annual SMB. Although the increasing summer precipitation are about 70.3, 51.9, and 8.5

244   mm, accounting for 83.9 %, 76.7 %, and 130.2 % for the annual precipitation, precipitation is mainly categorized as liquid in

245   the model due to that the average summer temperature was about 6.6 °C during LIA, larger than 2 °C (Eq. 1). Thus, glacier

246   accumulation is less during the summer. On the other hand, the summer temperature decreased about -0.9, -1.2, and -0.3 °C

247   for these three experiments, respectively. The reduced summer temperature decreased the cumulative positive temperature,

248   resulting in the reduction in summer ablation (Eq. 1). The SMB is determined by both the ablation and the accumulation (Peng

249   et al., 2020). Although the accumulation did not change too much in summer, the low summer temperature reduces the ablation,

250   resulting in an increase in the SMB of glaciers.

251
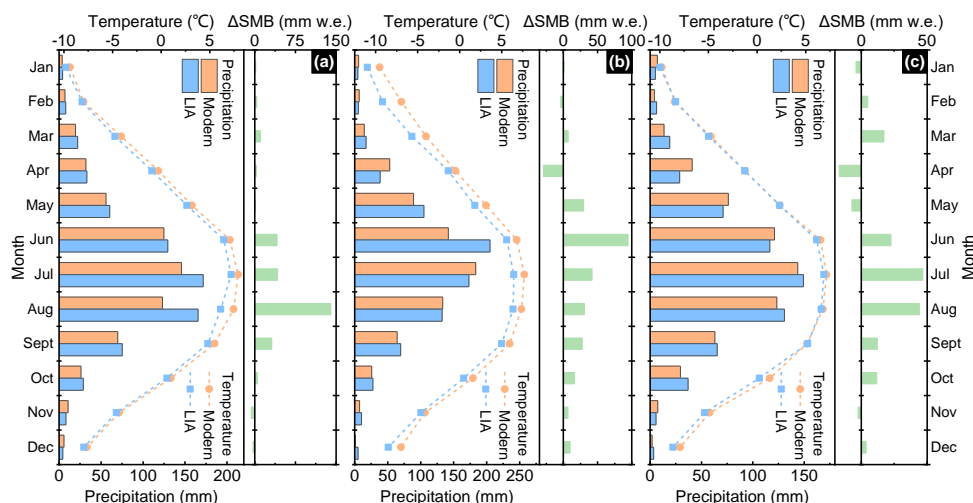
Figure 4. The average monthly temperature, precipitation, and ΔSMB during LIA (from LIA-4 to LIA-1) and modern (1950s) of (a) GISS, (b) IPSL, and (c) MPI.

We also conducted the sensitivity analysis to examine the influence of seasonal temperature or precipitation on glacier change (Fig. 5). Glaciers shrink gradually in response to increasing annual temperature from 0.1 to 0.4 ℃ and disappear after the annual temperature is larger than 0.5 ℃ or after the summer temperature larger than 0.8 ℃. The regional averaged glacier length increases linearly when the annual temperature decreases from 0.1 to 1.0 ℃, with an average rate of 1600 m/℃. Applying the same simulation strategy, the change rates of glacier length due to the temperature decreasing in spring, summer, autumn, and winter are estimated as 82, 1008, 602, and 0 m/℃, respectively, account for 5 %, 63 %, 38 %, and 0 % of the annual change. These results confirm that the temperature changes in summer and autumn seasons explain >90 % variance of the changes in glacier length.

When forced by an increase of present-day annual precipitation of 2 % to 20 % with keeping temperature fixed, the model, predicts an increase of the glacier length by 31 m per % precipitation increase. For seasonal precipitation changes from 102 to 120 % of present-day values, the changes in glacier length are higher in spring (18 m/%) and autumn (12 m/%), followed by winter (5 m/%) and summer (2 m/%). Therefore, the precipitation increases in the spring and autumn have more influences on glacier changes.

Based on the seasonal temperature changes (Fig. 4) for the GISS, IPSL, and MPI experiments and the glacier length change sensitivity to temperature mentioned above, the glacier length increased about 187.1 %, 267.5 %, 91.0 % longer than the present (672 m), respectively. Similarly, the glacier length increased about 35.2 %, 37.2 %, 1.2 % for the GISS, IPSL, and MPI experiments, respectively. Compared with the glacier length change caused by seasonal temperature and precipitation change, we argue that the change in temperature, especially summer temperature, is the dominant forcing factor for glacier changes during the LIA. In contrast, the impact of precipitation change is limited. In addition, the amplitude of glacier length change is larger for the steady-state simulation than that for the continuous simulation because the glacial response to climate

275   change always takes thousands of years, or even longer, during which the climate has become warm.

276
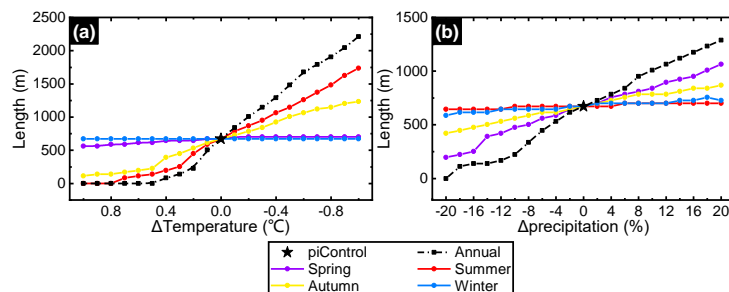
277

278   **Figure 5. Sensitivity of glacier length to annual or seasonal (a) temperature and (b) precipitation perturbations.**

279   **5 Conclusions**

280   We simulated the glacial evolution across BH over the past millennium using the coupled mass-balance and ice flow

281   model, OGGM. Compared with the geomorphological maps and ^{10}Be exposure ages, OGGM broadly captures the amplitude

282   of glacier length changes, especially for the GISS climate datasets. The ELA changes driven by MPI climate dataset are

283   consistent with the regional averaged ΔELA nearby BH, but the model overestimates ΔELA for GISS and IPSL experiments.

284   In addition, OGGM overestimates glacier extent in a factor of >2 due to the limitation of the model.

285   Four LIA substages were identified at about 1270s-1400s, 1470s-1520s, 1700s-1710s, and 1820s-1900s (from LIA-4 to

286   LIA-1) based on the simulations. The IPSL dataset is better to reconstruct the pattern of glacier changes in BH. The most and

287   second extensive glacial advances occurred during LIA-4 and LIA-2 for the IPSL experiment, consistent with regional glacial

288   chronological and geomorphic evidence. The number of the substages for individual glacier has a negative correlation with

289   glacier length, and the amplitude of length change for each glacier is also varying from different features of glaciers. The

290   regional pattern of glacier changes represented the characteristics of most glaciers.

291   The glacier advances are dominated by the reduction of summer ablation. Specifically, glaciers were more sensitive to the

292   changes in the summer and autumn temperature or the spring and autumn precipitation in BH.

293   Although limitations still exist in the simulations, such as the application of OGGM on glacier area and volume changes,

294   this study presented the first simulation of sub-millennium glacial evolutions during LIA in BH using the OGGM. We also

295   found a testable relationship between seasonal climate change and glacier expansion. Our findings provide important insights

296   into the climate forcing mechanism on glacier change at centennial timescale. The evaluation of the effects of different climate

297   datasets on glacier change helps choose the suitable climate dataset for predicting the changes of glacier and water sources in

298   response to future climate change.

299   **Code and data availability.** Code to run OGGM v1.2 is available at https://doi.org/10.5281/zenodo.2580277 (Maussion et

300   al., 2019).

301   **Author contributions.** Study concept devised by CW. YW performed the model runs and analysis, and wrote the original

302   draft. LY and LG reviewed and revised the paper.

303   **Competing interests.** The authors declare that they have no conflicting interests.

304   **Acknowledgments.** This work was supported by the Second Tibetan Plateau Scientific Expedition and Research (STEP; grant
305   no. 2019QZKK0205) and the National Natural Science Foundation (NSFC; grant no. 41771005, 41371082).

306   **References**

307   Bahr, D. B., Pfeffer, W. T., and Kaser, G.: A review of volume-area scaling of glaciers. *Rev. Geophys.*, *53*, 95–140,

308   https://doi.org/10.1002/2014RG000470, 2015.

309   Balco, G., Stone, J.O., Lifton, N.A., and Dunai, T.J.: A complete and easily accessible means of calculating surface exposure

310   ages or erosion rates from ^{10}Be and ^{26}Al measurements, *Quat. Geochronol.*, *3*, 174-195,

311   https://doi.org/10.1016/j.quageo.2007.12.001, 2008.

312   Barnard, P.L., Owen, L.A., Finkel, R.C., and Asahi, K.: Landscape response to deglaciation in a high relief, monsoon-

313   influenced alpine environment, Langtang Himal, Nepal, *Quaternary. Sci. Rev.*, *25*, 2162-2176,

314   https://doi.org/10.1016/j.quascirev.2006.02.002, 2006.

315   Barnard, P.L., Owen, L.A., Sharma, M.C., and Finkel, R.C.: Late Quaternary (Holocene) landscape evolution of a monsoon-

316   influenced high Himalayan valley, Gori Ganga, Nanda Devi, NE Garhwal, *Geomorphology*, *61*, 91-110,

317   https://doi.org/10.1016/j.geomorph.2003.12.002, 2004.

318   Benn, D.I., and Lehmkuhl, F.: Mass balance and equilibrium-line altitudes of glaciers in high-mountain environments, *Quatern.*

319   *Int.*, *65/66*, 15-29, https://doi.org/10.1016/S1040-6182(99)00034-8, 2000.

320   Bueler, E., and Brown, J.: Shallow shelf approximation as a "sliding law" in a thermo mechanically coupled ice sheet model,

321   *J. Geophys. Res-Earth.*, *114*, F03008, https://doi.org/10.1029/2008JF001179, 2009.

322   Carrivick, J.L., Boston, C.M., King, W., James, W.H., Quincey, D.J., Smith, M.W., Grimes, M., and Evans, J.: Accelerated

323   volume loss in glacier ablation zones of NE Greenland, Little Ice Age to present, *Geophys. Res. Lett.*, *46*, 1476–1484,

324   https://doi.org/10.1029/2018GL081383, 2019.

325   Chandler, B.M.P., Boston, C.M., and Lukas, S.: A spatially-restricted Younger Dryas plateau icefield in the Gaick, Scotland:

326   Reconstruction and palaeoclimatic implications, *Quaternary. Sci. Rev.*, *211*, 107-135,

327   https://doi.org/10.1016/j.quascirev.2019.03.019, 2019.

328   Dortch, J.M., Owen, L.A., and Caffee, M.W.: Timing and climatic drivers for glaciation across semi-arid western Himalayan-

329   Tibetan orogen, *Quaternary. Sci. Rev.*, *78*, 188-208, http://dx.doi.org/10.1016/j.quascirev.2013.07.025, 2013.

330   Eis, J., Maussion, F., and Marzeion, B.: Initialization of a global glacier model based on present-day glacier geometry and past

331   climate information: an ensemble approach, *The Cryosphere*, *13*, 3317-3335, https://doi.org/10.5194/tc-13-3317-2019, 2019.

332   Farinotti, D., Brinkerhoff, D. J., Clarke, G. K. C., Füst, J. J., Frey, H., Gantayat, P., Gillet-Chaulet, F., Girard, C., Huss, M.,

333   Leclercq, P. W., Linsbauer, A., Machguth, H., Martin, C., Maussion, F., Morlighem, M., Mosbeux, C., Pandit, A., Portmann,

334   A., Rabatel, A., Ramsankaran, R., Reerink, T. J., Sanchez, O., Stentoft, P. A., Singh Kumari, S., van Pelt, W. J. J., Anderson,

335   B., Benham, T., Binder, D., Dowdeswell, J. A., Fischer, A., Helfricht, K., Kutuzov, S., Lavrentiev, I., McNabb, R.,

336   Gudmundsson, G. H., Li, H., and Andreassen, L. M.: How accurate are estimates of glacier ice thickness? Results from ITMIX,

337   the Ice Thickness Models Intercomparison eXperiment, The Cryosphere, 11, 949–970, https://doi.org/10.5194/tc-11-949-2017,

338   2017.

339   Fu, P., Stroeven, A.P., Harbor, J.M., Hättestrand, C., Heyman, J., Caffee, M.W., and Zhou, P.: Paleoglaciation of Shaluli Shan,

340   southeastern Tibetan Plateau, *Quaternary. Sci. Rev.*, *64*, 121-135, http://dx.doi.org/10.1016/j.quascirev.2012.12.009, 2013.

341   Goosse, H., Barriat, P-Y., Dalaiden, Q., Klein, F., Marzeion, B., Maussion, F., Pelucchi, P., and Vlug, A.: Testing the

342   consistency between changes in simulated climate and Alpine glacier length over the past millennium, *Clim. Past.*, *14*, 1119-

343   1133, https://doi.org/10.5194/cp-14-1119-2018, 2018.

344   Greve, R.: A continuum-mechanical formulation for shallow polythermal ice sheets. *Philos. T.R. Soc. A.*, *355*(1726), 921-974,

345   https://doi.org/10.1175/1520-0442(1997)010<0901:AOAPTD>2.0.CO;2, 1997a.

346   Greve, R.: Application of a polythermal three-dimensional ice sheet model to the Greenland ice sheet: Response to steady-

347   state and transient climate scenarios, *J. Climate.*, *10*(5), 901-918, https://doi.org/10.1098/rsta.1997.0050, 1997b.

348   Grove, J.M.: *Little Ice Age, 2 ed*, Routledge, 2013.

349   Heyman, J.: Paleoglaciation of the Tibetan Plateau and surrounding mountains based on exposure ages and ELA depression

350   estimates, *Quaternary. Sci. Rev.*, *91*, 30-41, http://dx.doi.org/10.1016/j.quascirev.2014.03.018, 2014.

351   Heyman, J., Stroeven, A.P., Harbor, J.M., and Caffee, M.W.: Too young or too old: Evaluating cosmogenic exposure dating

352   based on an analysis of compiled boulder exposure ages, *Earth. Planet. Sc. Lett.*, *302*, 71-80,

353   https://doi.org/10.1016/j.epsl.2010.11.040, 2011.

354   Li, Y., Liu, G., Kong, P., Harbor, J., Chen, Y., and Caffee, M.: Cosmogenic nuclide constraints on glacial chronology in the

355   source area of the Urumqi River, Tian Shan, China, *J. Quaternary. Sci*, *26*(3), 297-304, https://doi.or/10.1002/jqs.1454, 2011.

356   Lipscomb, W.H., Price, S.F., Hoffman, M.J., Leguy, G.R., Bennett, A.R., Bradley, S.L., Evans, K.J., Fyke, J.G., Kennedy, J.H.,

357   Perego, M., Ranken, D.M., Sacks, W.J., Salinger, A.G., Vargo, L.J., and Worley, P.J.: Description and evaluating of the

358   Community Ice Sheet Model (CISM) v2.1, *Geosci. Model. Dev.*, *12*, 387-424, https://doi.org/10.5194/gmd-12-387-2019, 2019.

359   Loibl, D., Lehmkuhl, F., and Grießinger, J.: Reconstructing glacier retreat since the Little Ice Age in SE Tibet by glacier

360   mapping and equilibrium line altitude calculation, *Geomorphology*, *214*, 22-39,

361   http://dx.doi.org/10.1016/j.geomorph.2014.03.018, 2014.

362   Liu, J., Yi, C., Li, Y., Bi, W., Zhang, Q., and Hu, G.: Glacial fluctuations around the Karola Pass, eastern Lhagoi Kangri Range,

363   since the Last Glacial Maximum, *J. Quaternary. Sci*, *32*(4), 516-527, https://doi.org/10.1002/jqs.2946, 2017.

364   Marzeion, B., Jarosch, A. H., and Hofer, M.: Past and future sea-level change from the surface mass balance of glaciers, *The*

365   *Cryosphere*, *6*, 1295–1322, https://doi.org/10.5194/tc-6-1295-2012, 2012.

366 Maussion, F., Butenko, A., Champollion, N., Dusch, M., Eis, J., Fourteau, K., Gregor, P., Jarosch, A. H., Landmann, J., Oesterle,

367 F., Recinos, B., Rothenpieler, T., Vlug, A., Wild, C. T., and Marzeion, B.: The Open Global Glacier Model (OGGM) v1.1,

368 Geosci. Model Dev., 12, 909–931, https://doi.org/10.5194/gmd-12-909-2019, 2019.

369 Murari, M.K., Owen, L.A., Dortch, J.M., Caffee, M.W., Dietsch, C., Fuchs, M., Haneberg, W.C., Sharma, M.C., and Townsend-

370 Small, A.: Timing and climatic drivers for glaciation across monsoon-influenced regions of the HimalayaneTibetan orogen,

371 *Quaternary Science Review*, *88*, 159-182, http://dx.doi.org/10.1016/j.quascirev.2014.01.013, 2014.

372 Oerlemans, J., Anderson, B., Hubbard, A., Huybrechts, Ph., Jóhannesson, T., Knap, W.H., Schmeits, M., Stroeven, A.P., van

373 de Wal, R.S.W., and Zuo, Z.: Modelling the response of glaciers to climate warming, *Climate Dynamics*, *14*, 267-274,

374 https://doi.org/10.1007/s003820050222, 1998.

375 Owen, L.A.: Latest Pleistocene and Holocene glacier fluctuations in the Himalaya and Tibet, *Quaternary. Sci. Rev.*, *28*, 2150-

376 2164, https://doi.org/10.1016/j.quascirev.2008.10.020, 2009.

377 Owen, L.A., and Dortch, J.M.: Nature and timing of Quaternary glaciation in the Himalayan-Tibetan orogen, *Quaternary. Sci.*

378 *Rev.*, *88*, 14-54, http://dx.doi.org/10.1016/j.quascirev.2013.11.016, 2014.

379 PAGES 2k-PMIP3 group.: Continental-scale temperature variability in PMIP3 simulations and PAGES 2k regional

380 temperature reconstructions over the past millennium, *Clim. Past.*, *11*, 1673-1699, https://doi.org/10.5194/cp-11-1673-2015,

381 2015.

382 Parkes, D., and Goosse, H.: Modelling regional glacier length changes over the last millennium using the Open Global Glacier

383 Model, *The Cryosphere*, *14*, 3135-3153, https://doi.org/10.5194/tc-14-3135-2020, 2020.

384 Pelto, B.M., Maussion, F., Menounos, B., Radić, V and Zeuner, M.: Bias-corrected estimates of glacier thickness in the

385 Columbia River Basin, Canada, *J. Glaciol*, *66*(260), 1051-1063, https://doi.org/10.1017/jog.2020.75, 2020.

386 Peng, X., Chen Y., Liu, G., Liu, B., Li, Y., Liu, Q., Han, Y., Yang, W., and Cui, Z.: Late Quaternary glaciations in the Cogarbu

387 valley, Bhutanese Himalaya, *J. Quaternary. Sci*, *34*(1), 40-50, http://dx.doi.org/10.1002/jqs.3079, 2019.

388 Peng, X., Chen, Y., Li, Y., Liu, B., Liu, Q., Yang, W., Liu, G.: Late Holocene glacier fluctuations in the Bhutanese Himalaya,

389 *Global. Planet. Change.*, *187*, 103137, https://doi.org/10.1016/j.gloplacha.2020.103137, 2020.

390 Qiao, B., and Yi, C.: Reconstruction of Little Ice Age glacier area and equilibrium line attitudes in the central and western

391 Himalaya, *Quatern. Int.*, *444*, 65-75, http://dx.doi.org/10.1016/j.quaint.2016.11.049, 2017.

392 Qureshi, M.A., Li, Y., Yi, C., and Xu, X.: Glacial changes in the Hunza Basin, western Karakoram, since the Little Ice Age,

393 *Palaeogeogr. Palaeocl.*, *562*, 110086, https://doi.org/10.1016/j.palaeo.2020.110086, 2021.

394 RGI Consortium.: Randolph Glacier Inventory (RGI)-A Dataset of Global Glacier Outlines: Version 6.0,

395 https://doi.org/10.7265/N5-RGI-60, 2017.

396 Saha, S., Owen, L.A., Orr, E.N., and Caffee, M.W.: High-frequency Holocene glacier fluctuations in the Himalayan-Tibetan

397 orogen, *Quaternary. Sci. Rev.*, *220*, 372-400, https://doi.org/10.1016/j.quascirev.2019.07.021, 2019.

398 Saha, S., Owen, L.A., Orr, E.N., & Caffee, M.W.: Timing and nature of Holocene glacier advances at the northwestern end of

399 the Himalayan-Tibetan orogen, *Quaternary. Sci. Rev.*, *187*, 177-202, https://doi.org/10.1016/j.quascirev.2018.03.009, 2018.

400 Schmidt, G. A., Jungclaus, J. H., Ammann, C. M., Bard, E., Braconnot, P., Crowley, T. J., Delaygue, G., Joos, F., Krivova,

401 N.A., Muscheler, R., Otto-Bliesner, B.L., Pongratz, J., Shindell, D.T., Solanki, S.K., Steinhilber, F., and Vieira, L.E.A.: Climate

402 forcing reconstructions for use in PMIP simulations of the last millennium (v1.0), *Geosci. Model. Dev.*, *4*, 33-45,

403 https://doi.org/10.5194/gmd-4-33-2011, 2011.

404 Solomina, O.N., Bradley, R.S., Hodgson, D.A., Ivy-Ochs, S., Jomelli, V., Mackintosh, A.N., Nesje, A., Owen, L.A., Wanner,

405 H., Wiles, G.C., and Young, N.E.: Holocene glacier fluctuations, *Quaternary. Sci. Rev.*, *111*, 9-34,

406 http://dx.doi.org/10.1016/j.quascirev.2014.11.018, 2015.

407 Taylor, K., Stouffer, R., and Meehl, G.: An Overview of CMIP5 and the Experiment Design, *B. Am. Meteorol. Soc.*, *93*, 485-

408 498, https://doi.org/10.1175/BAMS-D-11-00094.1, 2012.

409 Winkelmann, R., Martin, M.A., Haseloff, M., Albrecht, T., Bueler, E., Khroulev, C., and Levermann, A.: The Potsdam Parallel

410 Ice Sheet Model (PISM-PIK) – Part 1: Model description, *The Cryosphere*, *5*, 715-726, https://doi.org/10.5194/tc-5-715-2011,

411 2011.

412 Xu, X., Pan, B., Hu, E., Li, Y., and Liang, Y.: Responses of two branches of Glacier No. 1 to climate change from 1993 to

413 2005, Tianshan, China, *Quatern. Int.*, *236*, 143-150, https://doi.org/10.1016/j.quaint.2010.06.013, 2010.

414 Yan, Q., Owen, L. A., Wang, H., and Zhang, Z.: Climate constraints on glaciation over High-Mountain Asia during the last

415 glacial maximum, *Geophys. Res. Lett.*, *45*, 9024–9033, https://doi.org/10.1029/2018GL079168, 2018.

416 Yan, Q., Owen, L. A., Zhang, Z., Wang, H., Wei, T., Jiang, N., and Zhang, R.: Divergent evolution of glaciation across High-

417 Mountain Asia during the last four glacial-interglacial cycles, *Geophys. Res. Lett.*, *48*, e2021GL092411,

418 https://doi.org/10.1029/2021GL092411, 2021.

419 Yan, Q., Owen, L.A., Zhang, Z., Jiang, N., and Zhang, R.: Deciphering the evolution and forcing mechanisms of glaciation

420 over the Himalayan-Tibetan orogen during the past 20,000 years, *Earth. Planet. Sc. Lett.*, *541*, 116295,

421 https://doi.org/10.1016/j.epsl.2020.116295, 2020.

422 Zhang, Q., Yi, C., Dong, G., Fu, P., Wang, N., and Capolongo, D.: Quaternary glaciations in the Lopu Kangri area, central

423 Gangdise Mountains, southern Tibetan Plateau, *Quaternary. Sci. Rev.*, *201*, 470-482,

424 https://doi.org/10.1016/j.quascirev.2018.10.027, 2018a.

425 Zhang, Q., Yi, C., Fu, P., Wu, Y., Liu, J., and Wang, N.: Glacier change in the Gangdise Mountains, southern Tibet, since the

426 Little Ice Age, *Geomorphology*, *306*, 51-63, https://doi.org/10.1016/j.geomorph.2018.01.002, 2018b.